Two-dimensional Janus semiconductor BiTeCl and BiTeBr monolayers : a first-principles study on their tunable electronic properties via an electric field and mechanical strain

Two-dimensional Janus Semiconductors BiTeCl and BiTeBr monolayers: A first-principles study of the tunable electronic properties via electric field and mechanical strain

A. Bafekry,[1,2,*] S. Karbasizadeh,[3] C. Stampfl,[4] M. Faraji,[5] D. M. Hoat,[6,7] I. Abdolhosseini Sarsari,[3] S.A.H Feghhi,[1] and M. Ghergherehchi[8]

[1]*Department of Radiation Application, Shahid Beheshti University, Tehran, Iran*
[2]*Department of Physics, University of Antwerp, Groenenborgerlaan 171, B-2020 Antwerp, Belgium*
[3]*Department of Physics, Isfahan University of Technology, Isfahan, 84156-83111, Iran*
[4]*School of Physics, The University of Sydney, New South Wales 2006, Australia*
[5]*Micro and Nanotechnology Graduate Program, TOBB University of Economics and Technology, Sogutozu Caddesi No 43 Sogutozu, 06560, Ankara, Turkey*
[6]*Institute of Theoretical and Applied Research, Duy Tan University, Ha Noi 100000, Viet Nam*
[7]*Faculty of Natural Sciences, Duy Tan University, Da Nang 550000, Viet Nam*
[8]*Department of Electrical and Computer Engineering, Sungkyunkwan University, 16419 Suwon, Korea*

Motivated by the recent successful synthesis of highly crystalline ultrathin BiTeCl and BiTeBr layered sheets [Debarati Hajra et al., ACS Nano 14, 15626 (2020)], herein for the first time, we carry out a comprehensive study of structural and electronic properties of the BiTeCl and BiTeBr Janus monolayers using density functional theory (DFT) calculations. Different structural and electronic parameters including lattice constant, bond lengths, layer thickness in the z-direction, different interatomic angles, work function, charge density difference, cohesive energy and Rashba coefficients are determined to provide a deep understanding of these monolayers. Calculations show good stability of the studied single layers. BiTeCl and BiTeBr monolayers are semiconductors with electronic bandgaps of 0.83 and 0.80 eV, respectively. Results also show that the semiconductor-metal transformation can be induced by increasing the number of layers. In addition, the engineering of the electronic structure is also studied by applying an electric field, and mechanical uniaxial and biaxial strain. Results show a significant change of the bandgaps and an indirect-direct band-gap transition can be induced. This study highlights the positive prospect for the application of BiTeCl and BiTeBr layered sheets in novel electronic and energy conversion systems.

I. INTRODUCTION

Two-dimensional (2D) nanosheet materials have become one of the most promising research fields in nanodevices and materials science[1] since the discovery of graphene.[2] During the last couple of decades, new 2D nanosheets have been developed, such as group IV monochalcogenides,[3] black phosphorous-like group VA elements,[4] Mxenes,[5] transition metal dichalcogenides,[6–9] graphene,[10] and so on. Most of these 2D materials demonstrate tunable electronic properties, e.g., the transition from semiconducting to metallic upon increasing layer number, and hence the electrical, optical and catalytic properties of the structure become layer dependent.[11–15] Due to the tunable electronic and layer-dependent properties, these 2D materials can absorb light in the spectrum ranging from ultraviolet (UV) to infrared (IR) regions.

Recently, the non-centrosymmetric Janus Rashba semiconductors with the general formula of ABX (where A is attributed to As, Sb, Bi; B= S, Se, Te; and X=Cl, Br, I) are of interest because of their versatile quantum phases.[16] The Janus sublayers consist of individual chalcogen, metal, and halogen atomic layers stacked together and separated by a weak van der Waals (vdW) force in triple-layers. The mentioned atomic structure induces a large built-in electric field and charge-separation in each Janus layer and along the stacking direction, respectively. The presence of a heavy Bi atom induces spin-orbit coupling (SOC) as predicted experimentally and theoretically in surface and bulk structures.[17] Intriguingly, the properties of one layer of the Janus Rashba semiconductors make them a perfect candidate for studying the interplay of contrasting quantum phenomena in a single layer material and optoelectronic and spintronic applications. Additionally, they have shown phase stability and continuous tunability based on Earth-abundant materials.[18] The method of annealing at high temperature has been used to fabricate BiSeCl,[19] BiSeI,[20] BiTeCl,[21] BiTeBr,[22] BiTeI[23] and AsSI[24] Janus Rashba semiconductors.

C. Xin et al.[25] investigated 2D SnS nanosheet layers exfoliated from the black phosphorus-like α phase SnS, using first-principle calculations and considering SOC. The electronic structures of bulk and 1-6 layers of SnS were calculated. Interestingly, due to the symmetry variation and a different splitting of the energy bands, the SnS nanosheet layers demonstrated an odd-even quantum confinement effect without any band gap reduction in different layer thicknesses. More significantly, such 2D SnS nanosheets also exhibited high mobility and high in-plane anisotropy, even better than black phosphorous. The high carrier mobility and size-dependent band gap of SnS make it a very promising candidate for optoelectronic applications. Z-Y. Zhao and Q-L. Liu[26] reported layer-dependent optical and electronic properties, and

the microstructure of $1T'$/2H/3R-MoS_2 nanosheets with different layer thicknesses, using first-principle calculations. The microstructure and weak van der Waals interaction are negligible in the evolution process from the monolayer to bulk. The variation of the van der Waals energy, binding energy, cleaving energy, and surface energy concerning the layer number were very slight. Here, the variation of layer spacing, bond length, and layer thickness concerning the layer numbers were neglected. From the monolayer to the bilayer, and then bulk, the E-K dispersion and the band structure were retained similarly. The soft variations have been depicted in the energy level degeneration, energy level shift, and the change of energy levels near the Fermi level. For the 2H-MoS_2 structure, the bandgap increased as the layer number decreased from bulk to 1 monolayer. Moreover, for layer numbers larger than 2, bilayer and monolayer $1T'$-MoS_2 nanosheet structures showed metallic, semi-metallic, and semiconductor conductivity, respectively. These variations confirmed that the electronic properties of MoS_2 nanolayers are strongly dependent upon the number of layers and interlayer separation. A variation of the optical properties of the nanosheets was also observed, which could be understood based on the electronic structure variation.

Very recently, new members of mono-elemental 2D lattices were successfully synthesized, namely 2D layered BiTeBr and BiTeCl employing a nanoscale conversion procedure.[27] The experimental study has confirmed that Janus semiconductors BiTeX (X=Cl, Br, I) can be manufactured in a few triple layers. on the other hand, regular Raman, EDX, SEM, and XRD show that highly crystalline BiTeBr and BiTeCl sheets can be fabricated on request. This work marks the direct deposition of BiTeX (X=Cl, Br, I) Rashba materials and offers ways to produce other Janus compounds belonging to MXY family members, where MXY (M = Bi, Sb X = Se, and Te, and X = Cl, Br, I).

In this paper, we report the structural and electronic properties of the 2D BiTeCl monolayer and the 2D BiTeBr structure from monolayer to multilayer utilizing first-principles calculations. Motivated by the exciting experimental realization of BiTeBr and BiTeCl, in this study our objective is to effectively explore the structural and electronic properties of these monolayers and multilayers using *ab initio* computational techniques. With this objective, effects of uniaxial and biaxial mechanical strain and electric field are also reported thoroughly in this article. Application of compressive and tensile strain on the structures can be of utmost importance, as the construction process of these layers can change the lattice constants and knowing how their properties change under these circumstances becomes mandatory. For applications such as optoelectronics, tuning the characteristics of BiTeBr and BiTeCl monolayers can be ultimately very valuable.

II. METHOD

First-principles calculations are carried out using the Vienna *ab initio* simulation package (VASP),[29,30] which is based on density functional theory (DFT).[33,34] The projector augmented wave (PAW)[35,36] method is used alongside plane-wave pseudopotentials to solve the Kohn-Sham equations and the exchange-correlation functional is described by the generalized gradient approximation (GGA) developed by Perdew, Burke and Ernzerhof.[31] The cutoff energy for the calculations is 600 eV to achieve accurate results regarding the description of the electronic properties. Structure optimization is performed until the Hellman-Feynman forces on each atom are less than 10^{-3} eV/Å, while the energy convergence threshold is 10^{-6} eV. To sample the first Brillouin zone (BZ), a dense gamma-centered k-point grid of 11×11×1 is used for the monolayer and few layers of BiTeBr; while a mesh of 10×10×1 is used for the structures of BiTeCl. The spin-orbit interaction is included in the calculations, the reason for it being the strong Rashba spin splitting. Under the assumption that the forces between the two layers of BiTeBr and BiTeCl in their few-layered forms are of van der Waals origin, the Grimme's DFT-D3 approach[37] is employed. To avoid any kind of spurious interaction between the layers in the z-direction, a large vacuum region of 20 Å suffices for all monolayer calculations, while the calculations involving two, three and four layers have this region at 25 Å, 35 Å and 45 Å, respectively.

III. STRUCTURAL PROPERTIES

The geometrical atomic structures of the BiTeCl and BiTeBr monolayers for different views are shown in Fig. 1(a). Notice that within the unit cell a Bi atom is located between one Te atom and one X (X=Cl and Br) atom, thus forming a monolayer with three kinds of atoms. The calculated lattice constants of the studied monolayers are 4.31 Å (BiTeCl) and 4.35 Å (BiTeBr). The bond lengths, Bi-Te (d_1) and Bi-X (d_2), are determined to be, respectively: 3.05 Å and 2.96 Å (BiTeCl), 3.06 Å and 3.10 Å (BiTeBr). The two angles of Bi-X-Bi and Bi-Te-Bi in the lattice of BiTeCl and BiTeBr are 93/89° and 89/90°, strongly deviating from 120° and indicating the in-plane anisotropy of the lattice. The thickness of BiTeCl and BiTeBr monolayers are determined to be 3.38 and 3.57 Å, respectively. The structural parameters including bond lengths and bond angles, as well as the calculated lattice constant of the hexagonal unit cells, are listed in Table I.

The dynamical stability of single-layers of BiTeX is verified by calculating their phonon band dispersions through the whole BZ which are presented in Figs. 1(b). The phonon branches are free from any imaginary frequencies indicating this fact for the structures. The work function is calculated using the following, $\Phi = E_{vacuum} - E_F$. The calculated work function for BiTeCl and BiTeBr monolayers are 5.17 and 4.94 eV, respec-

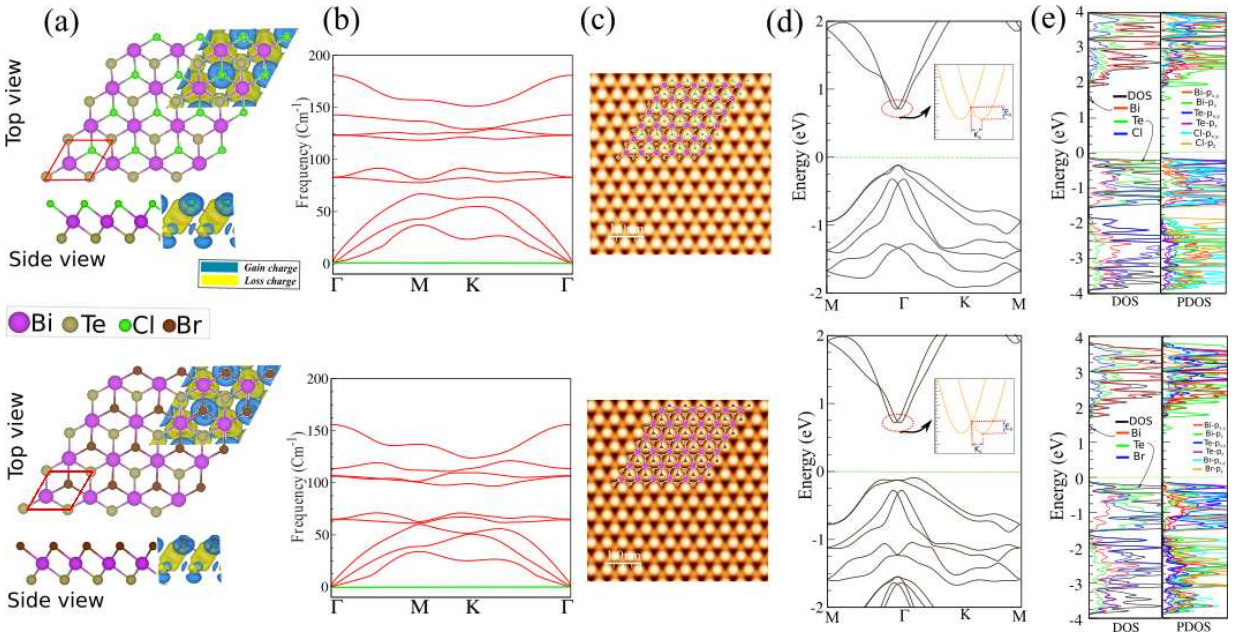

Figure 1. (a) Atomic structures and the difference in charge density, (b) phonon dispersion, (c) simulated STM image, (d) electronic band structures using PBE+SOC and (e) the corresponding DOS and PDOS of BiTeCl (top) and BiTeBr (bottom) monolayers. The primitive unit cell is indicated in (a) by a red parallelogram. The zero of energy is set to the Fermi-level.

Table I. Structural and electronic parameters of the BiTe (X=Cl, Br) monolayers including: lattice constants a; bond lengths between the Bi-Te (d_1) and Bi-X (d_2) atoms, bond angles between Bi-X-Bi (θ_1) and Bi-Te-Bi (θ_1) atoms, thickness, defined by the difference between the largest and smallest z coordinates of the X and Te atoms (t), cohesive energy per atom, (E_{coh}), charge transfer (ΔQ) between atoms, work function (Φ), band gap (E_g) (PBE with SOC) and Rashba coefficients are shown.

	a (Å)	d_1 (Å)	d_2 (Å)	t (Å)	$\theta_{1,2}$ (°)	E_{coh} (eV/atom)	ΔQ (e)	Φ (eV)	E_g (eV)	E_R (eV)	k_0 (Å^{-1})	α_R (eV.Å)
BiTeCl	4.31	3.05	2.96	3.38	93,89	-7.94	0.75 (0.82)	5.17	0.83	0.015	0.0039	7.48
BiTeBr	4.35	3.06	3.10	3.57	89,90	-7.36	0.59 (0.64)	4.94	0.80	0.021	0.0046	9.15

tively.

The difference in charge density ($\Delta\rho$) is defined as: $\Delta\rho = \rho_{tot} - \rho_{Bi} - \rho_{Te} - \rho_X$ where ρ_{tot}, ρ_{Bi}, ρ_{Te} and ρ_X represent the charge densities of the BiTeX structure and isolated atoms, respectively. From the difference in charge density, we find that the positively charged Bi atoms are surrounded by negatively charged X atoms. Notice that each S, Se and Te atom, labeled 1(2) (see Fig. 1(b)), gains about 0.75(0.82)e, 0.59(0.64)e and 0.36 (0.37e from the adjacent Sb atoms in BiTeCl and BiTeBr, respectively.

The cohesive energy per atom is defined as: $E_{coh} = \frac{E_{tot} - E_X - E_{Bi} - E_{Te}}{3}$, where E_X, E_{Bi} and E_{Te} represent the energies of isolated single X (Cl and Br), Bi and Te atoms, respectively; and 3 is the total number of atoms in the unit cell. E_{tot} represents the total energy of the BiTeX monolayer. The cohesive energy of BiTeCl is found to be -7.94 eV/atom, while the cohesive energy of BiTeBr is obtained to be -7.36 eV/atom. These findings indicate that the formation of BiTeCl from free atoms is more favorable than BiTeBr.

The electronic band structures with the corresponding density of states (DOS) and partial DOS (PDOS) of the BiTeX monolayers are shown in Figs. 1(d) and (e). Our results show that the BiTeCl and BiTeBr monolayers are semiconductors, with indirect band gaps of 0.83 eV and 0.80 eV, respectively. These values are obtained taking into consideration the SOC. In addition, the valance band maximum (VBM) occurs along the $\Gamma - K - M$ direction, and the conduction band minimum (CBM) lies at the Γ-point. To understand the contribution of the different orbitals to the electronic states and the bonding characteristics, we carry out calculations of the DOS/PDOS as shown in Fig. 1(e). It is observed that the states near the Fermi-level have contributions from p orbitals of Bi and Te. The contributions from the p_z orbitals of Bi and Te are located significantly higher than that of $p_{x,y}$-orbitals. The fact that the p_z-orbitals are dominant is caused by the sp^3-like the bond of Bi and the sp^2-like the bond of Te forming the BiTeX.

The Rashba coefficients for each structure is computed through the shape of each band structure. As is shown in

Fig. 1(d), k_0 is the distance between CBM and the lowest spot of the empty bands at Γ-point and is called the momentum offset. E_R, or the energy splitting, is also computable from the band structure and is the energy difference between the two aforementioned locations. The simplified formulas for the calculation of k_0 and E_R are as follow:

$$E_R = \frac{\hbar^2 k_0^2}{2m^*}, k_0 = \frac{m^* \alpha_R}{\hbar^2}; \quad (1)$$

where α_R is the coupling constant. This parameter is obtainable via the relationship between k_0 and E_R, where

$$\alpha_R = \frac{2E_R}{k_0}. \quad (2)$$

The Rashba coefficients obtained for the BiTeBr and BiTeCl monolayers are listed in Table I. The coupling constant (α_R) for both monolayers is more than sufficient for application in spintronics.

IV. BITEX MULTILAYER

The electronic band structures of one to four layers of BiTeBr are presented in Fig. 2(b). As pointed out before, the BiTeBr monolayer is a semiconductor with a bandgap of 0.80 eV. Through creating the bilayer of BiTeBr, the bandgap is reduced to 0.22 eV using PBE+SOC. The forces between the layers are determined as van der Waals weak interactions and the distance between the two layers is3.10 Å. Upon adding another layer, the bandgap of the structure is reduced to zero and a transition from semiconductor to metal takes place. This metallic state remains, even after four layers of BiTeBr are stacked together. The distance between layers remains at 3.10 Å. The corresponding total DOS of these BiTeBr band structures for one to four layers are shown in Fig. 2(c). As layers are added to the structure, the overlap of the bands and the presence of more states are visible. The same behavior is seen for BiTeCl in Fig. 2(a). The monolayer of BiTeCl has a bandgap of 0.83 eV, while its bilayer has a value of 0.17 eV. The same transition to metal occurs as more layers are added. The HSE+SOC density of state calculations as reported in Fig. S2 of the supplementary information confirm the metallic nature for three layers. The distance between the layers is calculated to be 2.99 Å after atomic relaxation.

V. ELECTRIC FIELD

The electronic band structure of BiTeCl and BiTeBr monolayers under the influence of different electric fields are shown in Figs. 3(a) and (b), respectively. An electric field is applied in the range of 0 to 1 V/Å in the parallel and antiparallel directions and the bandgap of each monolayer is given in Fig. 3(d). The application of a parallel electric field causes an increase in the bandgap for both BiTeCl and BiTeBr. The bandgap of BiTeCl reaches zero as the electric field in the parallel direction goes to 0.8 V/Å. Analogous behaviour occurs for BiTeBr at 0.9 V/Å where the monolayer transforms to a metal. On the other hand, when an antiparallel electric field is applied, both the bandgaps of BiTeCl and BiTeBr increase. This continues for BiTeBr until the field reaches 0.4 V/Å where the bandgap begins a gradual decline then starts to fall steeply as it reaches 0.7 V/Å. At 0.9 V/Å, the bandgap no longer exists and BiTeBr has become a metal. Analogous behaviour occurs for BiTeCl, with some minor differences. When BiTeCl is subject to an antiparallel electric field, the gradual decline begins at 0.5 V/Å, the steep variation starts at 0.8 V/Å, and for even greater values of electric field than 1 V/Å, the system does not transform to a metallic state. On inspection of the band structures, we can see that both VBM

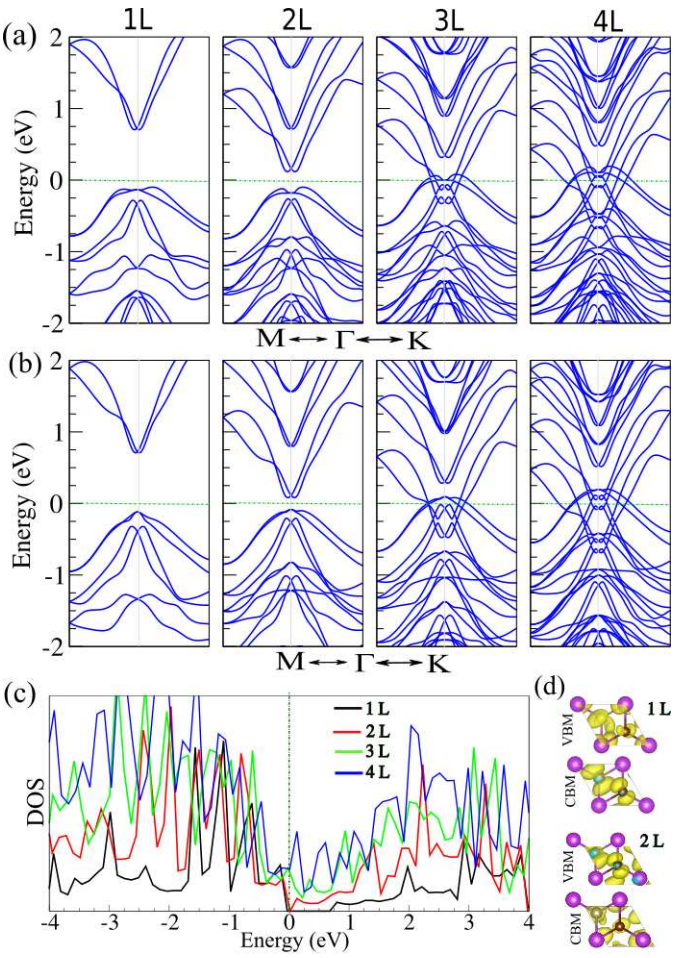

Figure 2. Electronic structure of few layer (a) BiTeCl and (b) BiTeBr as function of layer thickness. (c) DOS of BiTeBr multilayers. (d) Charge density of the state at the VBM and CBM of the BiTeBr monolayer and bilayer. The zero of energy is set to the Fermi level.

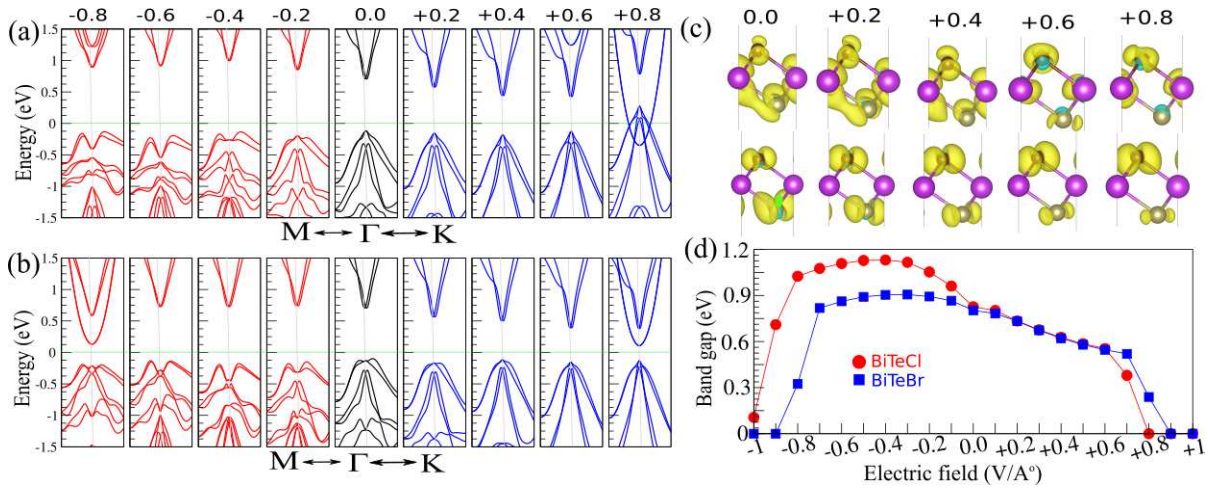

Figure 3. Electronic band structures of (a) BiTeCl and (b) BiTeBr monolayers, as a function of applied electric field in the parallel (right) and anti-parallel (left) directions. The positive (negative) electric field refers to parallel (antiparallel) to the z-axis in the normal direction, where the strength of fields vary from 0 to 1 V/Å. The energy is given relative to the Fermi energy. (c) The electron charge density of the VBM and CBM of the BiTeBr monolayer for different strengths of E-field. (d) Variation of bandgap as a function of applied electric field.

and CBM shift to theΓ point when switching the electric field from antiparallel to parallel, causing an indirect-direct band gap transition. Note that for both studied monolayers, this transition is reached from anti parallel strength of +0.4 (V/Å).

Due to the relative similarity between BiTeBr and BiTeCl, the electric field is only applied to the bilayer of BiTeBr. The range of this field, which again is in both parallel and antiparallel directions, is less than what was applied to the monolayers, as the changes in this structure are much more drastic. Fig. 4 shows the electronic band structures of BiTeBr bilayer for applied electric fields in the range of 0 to 0.3 V/Å. The changes of the bandgap quite markedly through the application of the parallel electric field. Application of an antiparallel electric field leads to metallic behavior of the BiTeBr bilayer. For a parallel field of +0.1 V/Å the bandgap decreases slightly, while the bandgap is considerably opened when the magnitude is +0.2 V/Å. Increasing the parallel field to +0.3 V//Å, an opposite variation is induced, reducing again the energy gap.

The Rashba coefficient α_R is proportional to the electric field for free electrons but has a more complex dependence for electrons in the solid. Thus the electric field changes the Rashba effect in two ways: first, by changing the density of the 2DEG in the surface layers, and second, by altering the surface asymmetry field ϵ and reorienting the orbital energies.[39] This effect, however, is not significant enough to alter the Rashba coefficients in a tangible way and is therefore, not dissected for this part.

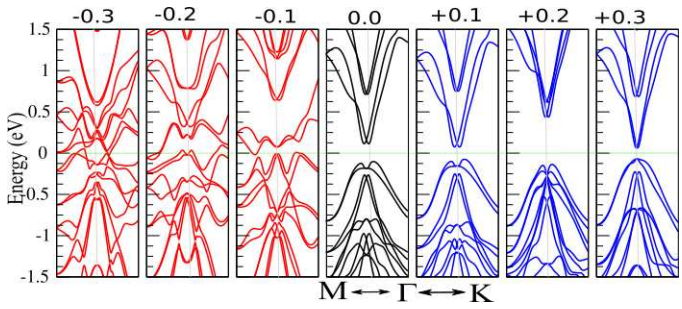

Figure 4. Electronic band structures of the BiTeBr bilayer, as a function of applied electric field in the parallel (right) and anti-parallel (left) directions. The positive (negative) electric field refers to parallel (antiparallel) to the z-axis in the normal direction, where the strength of fields varies from 0 to 0.3 V/Å. The energy is calculated relative to the Fermi energy.

VI. MECHANICAL STRAIN

Uniaxial and biaxial, compressive and tensile strain in the range of 0 to 6% is applied to BiTeBr and BiTeCl monolayers. Fig. 5(a) shows the electronic band structure of the BiTeBr monolayer under the influence of uniaxial strain while Fig. 5(b) demonstrates this in the presence of biaxial strain in 2% intervals. The electronic band structure of the BiTeCl monolayer under the influence of uniaxial strain Fig. S1 of the supplementary information. It is observed that the splitting of the VBM and CBM disappears with the increase of the compressive strain and becomes greater with increasing tensile strain. Fig. 5(c) shows the bandgap variation with both compressive and tensile strain for both the BiTeBr and BiTeCl monolayers. We only show the band structures of one of the monolayers, as no substantially different

behaviour occurred in the bands of BiTeCl. Upon applying uniaxial tensile strain to the monolayer of BiTeBr, the value of the bandgap starts to decrease reaching 0.58 eV at 6%. When the strain is compressive, there is little variation until the 2%, after which the bandgap decreases and reaches 0.69 eV at 6%. For biaxial tensile strain, the decline is steeper, with the bandgap reaching 0.47 eV at 6%. For compressive strain, the bandgap increases slightly, becoming 0.84 eV at 1%. After that, it stays almost constant up to 6%. Very similar behavior is seen for the monolayer of BiTeCl. Opposite to the behaviour of the uniaxial tensile strain for BiTeBr, BiTeCl sees a small increase at 1% and then goes on to decrease steadily until reaching the value of 0.66 eV at 6%. The behaviour under compressive strain closely follows that already seen in BiTeBr. The same is true for the biaxial compressive strain, where the two structures are equally flat on reaching 6% strain. The difference in BiTeCl is that this steadiness continues even after tensile strain is applied until it reaches 1%. After that, the steep decline starts and takes the bandgap to 0.46 eV at 6%. The overlap between interacting orbitals determines bandgap and bandwidth. Here, the biaxial compressive strains do not effect overlap between interacting orbitals as well as uniaxial compressive strain.

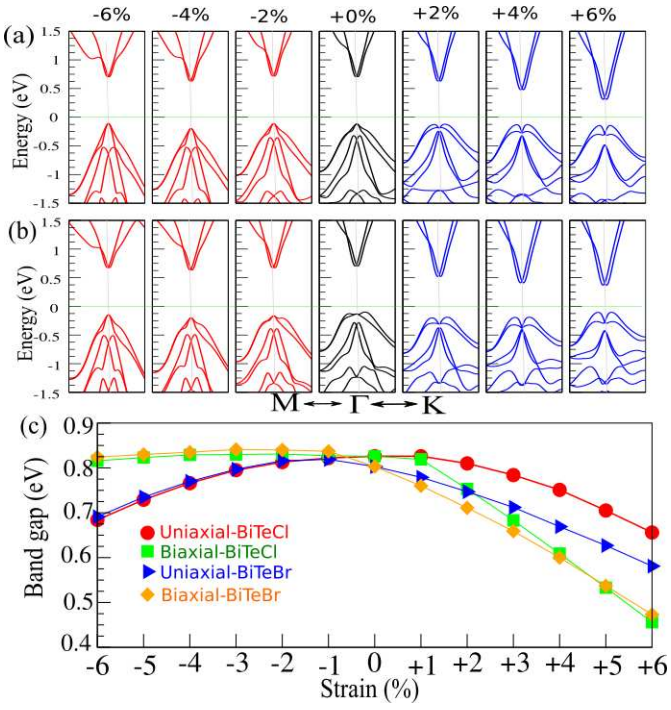

Figure 5. Electronic band structures of BiTeBr monolayer as a function of applied (a) uniaxial and (b) biaxial strain. Compressive (tensile) indicated in the left (right) of panel. The positive (negative) strain refers to tensile (compressive) direction, where the strength of fields varies from 0 to 6%. The energy is calculated relative to the Fermi energy. (c) Variation of the bandgap as a function of applied uniaxial and biaxial strain.

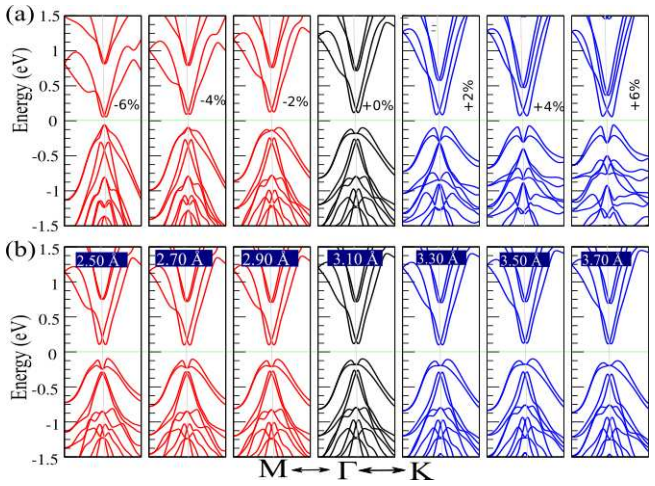

Figure 6. Electronic band structures of the BiTeBr bilayer, as a function of (a) applied biaxial strain and (b) interlayer distance. Compressive (tensile) biaxial strain is indicated in the left (right) of the panel. The positive (negative) strain refers to tensile (compressive) strain, where the strength of fields varies from 0 to 6%. The interlayer distance is changed in 0.2 Å intervals from the equilibrium position of the layers. The energy is calculated relative to the Fermi energy.

Biaxial, compressive and tensile, strain is also applied in the range of 0 to 6% to the bilayer of BiTeBr. Fig. 6(a) shows the electronic band structures of this bilayer in 2% intervals. The most notable change is the gradual disappearance of the VBM split under biaxial strain, while the band structure exhibits quite similar profiles for different interlayer distances. The changes in the bandgap value as a result of this strain, for both compressive and tensile, are very small and they both have the same effect on the bandgap as it decreases both ways. Tensile strain reduces the bandgap to 0.12 eV at 6%, while compressive strain yields a bandgap of 0.11 eV at 6%. Electronic band structures of bilayer BiTeBr are given for different interlayer distances in Fig. 6(b). As mentioned before, the most stable structure of the BiTeBr bilayer has a separation distance of 3.10 Å. This distance is increased and decreased at 0.1 Å intervals, going as far as 3.70 Å and 2.50 Å, respectively. As the interlayer distance increases, so does the value of the bandgap, reaching 0.24 eV when the distance is 3.70 Å. When the separation between the layers decreases, the bandgap decreases and is 0.20 eV at 2.50 Å. The overall change of the bandgap value, however, is not very substantial; just 0.04 eV change for a change of the interlayer distance in the range of 1.2 Å.

Although the bandgap of the BiTeBr bilayer does not change drastically or interestingly when modified with biaxial strain or interlayer distance, another parameter sees a considerable variance. The Rashba coefficients are seen to differ quite markedly when biaxial strain is applied or the interlayer distance is changed. The CBMs of both BiTeBr and BiTeCl systems are formed directly from Bi-pz orbitals. These orbitals form an anti-bonding

Table II. Rashba coefficients as a function of interlayer distance and biaxial strain in bilayer BiTeBr. E_R, k_0 and α_R are written in a range of 0 to 6% of biaxial strain in 2% intervals and interlayer distance that reaches 0.6 Å further from the equilibrium position of the layers, both ways.

Biaxial Strain	-6%	-4%	-2%	0%	2%	4%	6%
E_R(eV)	0.023	0.030	0.039	0.044	0.062	0.078	0.101
k_0(Å^{-1})	0.0049	0.0063	0.0071	0.0082	0.0106	0.0134	0.0160
α_R(eV.Å)	9.53	9.60	11.02	10.74	11.75	11.72	12.57
Interlayer Distance	2.50Å	2.70Å	2.90Å	3.10Å	3.30Å	3.50Å	3.70Å
E_R(eV)	0.098	0.079	0.059	0.044	0.034	0.028	0.025
k_0(Å^{-1})	0.0109	0.0101	0.0094	0.0082	0.0070	0.0062	0.0055
α_R(eV.Å)	17.96	15.63	12.64	10.74	9.71	9.10	9.26

state, which is created by the overlap of the electronic wave functions; and as a result of this overlap, spin splitting occurs in the conduction band near the Γ point. This overlap only intensifies as tensile strain is applied to the structure, which sees a change in the splitting and in turn, the Rashba coefficients. The opposite happens as compressive strain is put on the device. Vertical strain or the differing of the interlayer distance manipulates the coefficients in the same way.[40] For the variation of the compressive strain of 6% to 6% tensile strain, the energy splitting (E_R) and momentum offset (k_0) increase, the result of which can be seen in the change in the value of the coupling constant (α_R). Changing the separation between the layers also has a direct effect on the Rashba coefficients, where E_R and k_0 increase with the layers closer together and decrease as the layers are pushed further away from each other. These coefficients are calculated and listed in Table II. The ability to tune these coefficients with such large variations can be highly effective in optoelectronic and spintronic applications.

VII. CONCLUSION

In summary, *ab initio* calculations have been used to investigate the structural and electronic properties of the recently synthesized 2D-BiTeX (X=Br, Cl) structures. Indirect bandgaps of 0.80 eV and 0.83 eV are obtained by PBE+SOC for BiTeBr and BiTeCl, respectively. Calculated phonon band dispersion shows dynamical stability of the 2D structures as they lack any imaginary frequencies. Two structures display splitting of the CBM because of the Rashba effect, with coupling constants (α_R) of 9.15 eV.Å and 7.48 eV.Å for BiTeBr and BiTeCl, respectively, which are well beyond requirements for future spintronic applications. By increasing the layer number, the bandgap exhibits a significant reduction and a metallic character is obtained from tri-layer and additional multilayer systems. Calculations show that the external electric field is effective to tune the electronic structure of BiTeCl and BiTeBr monolayers and bilayers, where the latter shows a stronger dependence. Additionally, the mechanical strain of both biaxial and uniaxial nature is quite effective in changing the bandgap of both monolayers. A quite small energy gap modification is induced by varying the interlayer distance. These factors mostly affect the Rashba coefficients with the coupling constant goes as far as 12.57 and 17.96 eV/Å, respectively. The results presented here provide valuable insight into the properties of BiTeBr and BiTeCl monolayer and multilayers, and their dependence on the strain, structure, and electric field, which is essential for their potential use in future applications and novel nanodevices.

VIII. ACKNOWLEDGMENTS

This work was supported by the National Research Foundation of Korea (NRF) grant funded by the Korea government (MSIT) (NRF-2015M2B2A4033123).

IX. DATA AVAILABILITY

The data that support the findings of this study are available from the corresponding author upon request.

* bafekry.asad@gmail.com

[1] Q. Tang, Z. Zhou, Prog. Mater. Sci. 2013, 58, 1244-1315.
[2] K. S. Novoselov, A. K. Geim, S. V. Morozov, D. Jiang, Y. Zhang, S. V. Dubonos, I. V. Grigorieva, A. A. Firsov, Sci. 2004, 306, 666-669.
[3] Y.Li, T. Ding, D.K. Sang, M. Wu, J. Li, C. Wang, F. Liu, H. Zhang, H. Xie, J. Mater. Chem. C, 2020,8, 4181-4191.
[4] S. Zhang, S. Guo, Z. Chen, Y. Wang, H. Gao, J. Gomez-Herrero, P. Ares, F. Zamora, Z. Zhu, H. Zeng, Chem. Soc. Rev. 2018, 47, 982-1021.

[5] Sh. Nyamdelger, T. Ochirkhuyag, D. Sangaa, D. Odkhuu, Phys. Chem. Chem. Phys., 2020,22, 5807-5818.

[6] S. Barja, S. Refaely-Abramson, B. Schuler, D. Y. Qiu, A. Pulkin, S. Wickenburg, H. Ryu, M. M. Ugeda, Ch. Kastl, Ch. Chen, Ch. Hwang, A. Schwartzberg, Sh. Aloni, S.-K. Mo, D. F. Ogletree, M. F. Crommie, O. V. Yazyev, S. G. Louie, J. B. Neaton, A. Weber-Bargioni , Nat. Commun. 10, 3382 (2019).

[7] P. Wang, Sh. Song, A. Najafi, Ch. Huai, P. Zhang, Y. Hou, Sh. Huang, Hao Zeng, ACS Nano 2020 14 (6), 7370-7379.

[8] J. Wang, H. Shu, T. Zhao, P. Liang, N. Wang, D. Cao, X. Chen, Phys. Chem. Chem. Phys., 2018,20, 18571-18578.

[9] M. Dou, M. Fyta, J. Mater. Chem. A, 2020,8, 23511-23518.

[10] M. Xu, T. Liang, M. Shi, H. Chen, Chem. Rev. 2013, 113, 3766-3798.

[11] Y-Q. Zhao, Q-R. Ma, B. Liu, Zh-Li. Yu, J. Yang, M-Q Cai, Nanoscale, 2018,10, 8677-8688.

[12] X. Fan, L. Su, F. Zhang, D. Huang, D. K. Sang, Y. Chen, Y. Li, F. Liu, J. Li, H. Zhang, H. Xie, ACS Appl. Mater. Inter. 2019 11 (50), 47197-47206.

[13] D. Kim, K. Park, F. Shojaei, T. Debela, K. Terfa, K. Ik Seon, S. In Hye, A. Jaemin, P. J. Pyoung, K. Jeunghee, H. Seok, J. Mater. Chem. A, 2019,7, 16526-16532.

[14] H. Shu, P. Luo, P. Liang, D. Cao, and X. Chen, ACS Appl. Mater. Inter. 2015 7 (14), 7534-7541.

[15] X. Niu, G. Wu, X. Zhang, J. Wang, Nanoscale, 2020,12, 6057-6063.

[16] H. Li, Y. Qin, B. Ko, D. B. Trivedi, D. Hajra, M. Y. Sayyad, L. Liu, S. H. Shim, H. Zhuang, S. Tongay, Adv. Mater. 2020, 32, 2002401.

[17] G. Landolt, S.V. Eremeev, O.E. Tereshchenko, S. Muff, B. Slomski, K.A. Kokh, M. Kobayashi, T. Schmitt, V. N. Strocov, J. Osterwalder, New J. Phys. 2013, 15, 085022.

[18] H. Kunioku, M. Higashi, R. Abe, Sci. Rep. 6, 32664 (2016).

[19] G. Voutsas, P. Rentzeperis, Z. Kristallogr. Cryst. Mater., 1986, 177, 117-124.

[20] M. Moroz and M. Prokhorenko, Inorg. Mater., 2016, 52, 765-769.

[21] C. Martin, A. Suslov, S. Buvaev, A. Hebard, P. Bugnon, H. Berger, A. Magrez and D. Tanner, Phys. Rev. B 2014, 90, 201204.

[22] A. Shevelkov, E. Dikarev, R. Shpanchenko and B. Popovkin, J. Solid State Chem., 1995, 114, 379-384.

[23] L. Wu, J. Yang, S. Wang, P. Wei, J. Yang, W. Zhang and L. Chen, Phys. Rev. B, 2014, 90, 195210.

[24] P. P. Seregin, V. P. Sivkov, F. S. Nasredinov, L. N. Vasilev, Y. V. Krylnikov and Y. P. Kostikov, Phys. Status Solidi A, 1977, 39, 437-444.

[25] C. Xin, J. Zheng, Y. Su, S. Li, B. Zhang, Y. Feng, F. Pan, J.Phys. Chem. C, 2016, 120, (39), 22663-22669.

[26] Z-Y. Zhao and Q-L. Liu, Catal. Sci. Technol., 2018,8, 1867-1879.

[27] D. Hajra, R. Sailus, M. Blei, K. Yumigeta, Y. Shen, S. Tongay, ACS Nano. 14 (2020) 15626?15632.

[28] Perdew, John P and Burke, Kieron and Ernzerhof, Matthias, Phys. Rev. Let., 77, (1996) 3865.

[29] G. Kresse and J. Hafner, Phys. Rev. B, 47 (1993), 558.

[30] G. Kresse and J. Furthmuller, Phys. rev. B, 54 (1996), 11169.

[31] J. P. Perdew, K. Burke, and M. Ernzerhof, Phys. Rev. Let., 77 (1996), 3865.

[32] D. Alfe, Comput. Phys. Commun., 180, (2009), 2622-2633,

[33] W. Kohn, and L. J. Sham, Phys. Rev., 140, (1965)

[34] P. Hohenberg, and W. Kohn, Phys. Rev., 136, (1964)

[35] P. E. Blöchl, Phys. Rev. B, 50 (1994), 17953

[36] G. Kresse, and D. Joubert, Phys. Rev. B, 59 (1999), 1758

[37] S Grimme, J Antony, S Ehrlich, H Krieg, The Journal of chemical physics 132 (15), 154104

[38] Yu A Bychkov and E I Rashba, Journal of Physics C: Solid State Physics, Volume 17, Number 33

[39] K. V. Shanavas and S. Satpathy, PRL 112, 086802 (2014)

[40] W. Yang, Z. Guan, H. Wang and J. Li, Phys. Chem. Chem. Phys., 23, 6552-6560 (2021)